# Independent-hot-spot approach to multibeam laser-plasma instabilities

R. K. Follett ⊙, H. Wen ⊙, D. H. Froula, D. Turnbull, and J. P. Palastro ⊙

*Laboratory for Laser Energetics, University of Rochester, 250 East River Road, Rochester, New York 14623, USA*

The independent-hot-spot model is used to develop an analytic formulation for multibeam laser-plasma instabilities in inhomogeneous plasmas. The model is applied to the absolute two-plasmon-decay instability and shows good agreement with simulations and experiments. The success of the model indicates the emergence of single-speckle behavior for sufficiently large speckles sizes.

In laser-driven inertial confinement fusion (ICF), a millimeter-scale cryogenic capsule of deuterium–tritium fuel with a thin outer ablator is imploded either by direct laser illumination (direct drive) or by focusing the lasers onto the interior walls of a hohlraum to generate an x-ray bath (indirect drive) [1]. In both cases, the many high-intensity laser beams overlapping in underdense plasma can drive various laser-plasma instabilities (LPIs) that can severely inhibit implosion performance [2,3].

Analytic results for instability behavior are typically limited to the case of a single plane-wave laser driving instability in the linear regime. ICF experiments, however, involve multiple overlapping laser beams, each using a phase plate that generates a complex speckle pattern in the plasma [4], and accurate predictions of instability behavior require a description that accounts for their combined interaction [5]. Multibeam interactions have historically been described using the common-wave model, where wave-vector matching considerations are used to show that overlapping laser beams can couple to a shared daughter wave propagating along the drive-beam axis of symmetry [6–11]. However, recent experiments and simulations of multibeam LPIs have shown that the common-wave description often fails to predict instability behavior [12–14].

In this Letter, we show that an independent-hot-spot model is the correct description of the two-plasmon-decay (TPD) instability in many cases where the common-wave model leads to inconsistencies with observations. A general prescription is developed for deriving independent-hot-spot models that is applied to the TPD instability and shows good agreement with multibeam simulations and experiments.

When discussing various models for instability behavior, we use the word *model* in the general sense of a conceptual model that is used to gain physical insight. A conceptual model can be used to derive a mathematical model that can be used to predict observables, but this is often unnecessary when sophisticated codes are available. Our goal here is to develop a framework for determining the correct conceptual model for interpreting multibeam LPI experiments.

Instability behavior in speckled beams can be divided into two categories: single-speckle and multispeckle. Single-

speckle behavior is when there is no communication between speckles, so the interaction within each speckle can be treated independently, and the global behavior can be treated statistically. The associated models for this behavior are referred to as independent-hot-spot models [15–22]. All instabilities exhibit single-speckle behavior in the limit of infinitely large speckles (the plane-wave limit), and multispeckle behavior emerges with decreasing speckle size. This categorization is useful because it makes it clear that the independent-hot-spot model is, by definition, the correct conceptual model for any instability exhibiting only single-speckle behavior. Any other model of instability behavior falls into the multispeckle category [23]. Consequently, the common-wave model is a multispeckle model (regardless of its predictive capability). We show below that TPD experiments are often in the single-speckle regime.

The speckle size plays a critical role in determining whether an instability is in the single- or multispeckle regime. For a single laser beam, the approximate speckle widths and lengths are $w_s = f_\# \lambda_0$ and $l_s = 2\pi f_\#^2 \lambda_0$, respectively, where $f_\#$ is the $f$-number and $\lambda_0$ is the wavelength (valid for $f_\# \gtrsim 1$) [24–26]. Multiple overlapping beams will have coherent structures over a range of spatial scales, but the highest intensities correspond to the coherent sum of all the incident beams, resulting in speckle sizes comparable to a single-beam aperture encompassing all of the beams [27]. Accordingly, for the purpose of predicting the properties of the highest-intensity speckles, a group of beams can be treated as a single large-aperture (small $f$-number) beam. Figure 1 shows the electric field of six $f/6.7$ beams incident at an angle of $\theta = 23°$ relative to the $x$-axis ($\lambda_0 = 0.405 \ \mu$m). The predominant coherent structures are ~0.4 $\mu$m wide and ~3 $\mu$m long, which is consistent with the effective $f$-number of the entire cone of beams given by $f_\# \approx 1/(2 \tan \theta) \approx 1.2$.

There is a straightforward procedure for constructing approximate analytic or semianalytic independent-hot-spot models by combining a model for the speckle statistics with a model for the single-speckle behavior. Given a collection of $N$ speckles, the absolute instability threshold occurs when the peak speckle intensity is equal to the single-speckle threshold, $I_M = I_{\text{thr,speckle}}$. Introducing the average laser intensity $I_0$
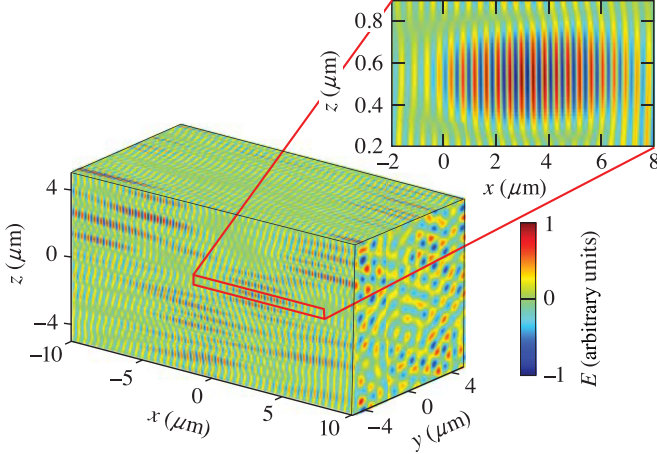
FIG. 1. Electric field for a six-beam cone of $f/6.7$ beams incident at $23°$ relative to the $x$ axis.

and ensemble averaging over speckle realizations, this can be written as

$$I_{\text{thr}} = \frac{1}{\langle I_M/I_0 \rangle} I_{\text{thr,speckle}}, \qquad (1)$$

where we have defined the expected average intensity at threshold $I_{\text{thr}} \equiv \langle I_0 \rangle$. Accordingly, evaluation of the expected threshold in the independent-hot-spot model is reduced to the evaluation of $\langle I_M/I_0 \rangle$ and $I_{\text{thr,speckle}}$.

The expected peak speckle intensity can be written in terms of the probability that every speckle intensity is less than $u$ [28]:

$$\langle I_M/I_0 \rangle = \int_0^\infty [1 - P(I/I_0 < u)^N] du. \qquad (2)$$

Reference [29] derives speckle distributions that are valid for high-intensity speckles ($I \gg I_0$) but are badly behaved at low intensities. Accordingly, we use exponential distributions at low intensities to generate probability distributions that are well behaved at all intensities:

$$P(I/I_0 > u)_{2D} = \begin{cases} e^{-u/\mu_2}, & u < u_{s2}, \\ A_2\left[\left(\frac{1}{2} + \frac{\pi}{4}\right)u + \frac{1}{2}\right]e^{-u}, & u > u_{s2}, \end{cases} \qquad (3)$$

$$P(I/I_0 > u)_{3D} = \begin{cases} e^{-u/\mu_3}, & u < u_{s3}, \\ A_3\left[u^{3/2} - \frac{3}{10}u^{1/2}\right]e^{-u}, & u > u_{s3}, \end{cases} \qquad (4)$$

where the $\mu_i$ are adjustable parameters and the $A_i$ and $u_{si}$ are chosen to make the distributions well-behaved (monotonically decreasing with continuous first derivative). Here $\mu_2 = \mu_3 = 4$ was chosen on the basis of comparison to simulations, which gives $A_2 = 1.185$, $u_{s2} = 0.944$, $A_3 = 1.848$, and $u_{s3} = 2.210$ (the results are only weakly sensitive to $\mu_i$ because it affects only the low-intensity part of the distribution).

Plugging Eqs. (3) and (4) into Eq. (2), using the binomial theorem, and integrating gives

$$\langle I_M/I_0 \rangle_{2D} = \sum_{a=1}^N \binom{N}{a}(-1)^a \left[ \frac{\mu_2}{a}(e^{-au_{s2}/\mu_2} - 1) \right.$$
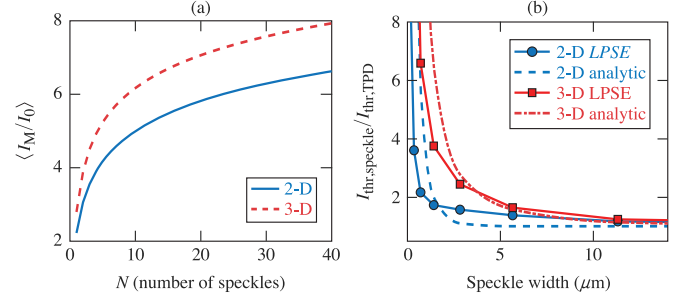$$\left. - A_2^a a^{-1-a} e^{\frac{2a}{2+\pi}} \left(\frac{2+\pi}{4}\right)^a \right.$$



FIG. 2. (a) The expected peak speckle intensities. (b) Single-speckle absolute TPD threshold as a function of speckle width.

$$\left. \times \Gamma\left(1 + a, \frac{2a}{2+\pi} + au_{s2}\right) \right], \qquad (5)$$

$$\langle I_M/I_0 \rangle_{3D} = \sum_{a=1}^N \binom{N}{a}(-1)^a \left[ \frac{\mu_3}{a}(e^{-au_{s3}/\mu_3} - 1) \right.$$
$$\left. - A_3^a \sum_{k=0}^a \binom{a}{k}\left(-\frac{3}{10}\right)^k a^{k-1-3a/2} \right.$$

$$\left. \times \Gamma(1 - k + 3a/2, au_{s3}) \right], \qquad (6)$$

where $\Gamma(s, x)$ is the incomplete gamma function. The expected peak speckle intensities [Eqs. (5) and (6)] are shown in Fig. 2(a). The expected peak intensity increases rapidly at small $N$ and grows logarithmically for large $N$ ($N \gtrsim 30$).

To determine $N$, we restrict our discussion to instabilities that are spatially localized by plasma inhomogeneity such that $N$ is the number of speckles in a cross section of the laser field (i.e., the interaction region is not significantly longer than the speckle length). Accordingly, $N$ is approximately the laser power divided by the mean power in a speckle, $N = P_L/\langle P_s \rangle$. The laser power is the average intensity times the cross-sectional area ($P_L = I_0\sigma_b$). To determine the mean power in a speckle, we first average over the probability density of speckle intensities to obtain the mean speckle intensity $\langle I/I_0 \rangle = \int_0^\infty uP(u)du$, where $P(u) = -\partial P(I/I_0 > u)/\partial u$. Equations (3) and (4) give

$$\langle I/I_0 \rangle_{2D} = \mu_2 - (\mu_2 + u_{s2})e^{-u_{s2}/\mu_2}$$
$$+ A_2 e^{-u_{s2}}[4 + \pi + (4 + \pi)u_{s2} + (2 + \pi)u_{s2}^2]/4, \qquad (7)$$

$$\langle I/I_0 \rangle_{3D} = \mu_3 - (\mu_3 + u_{s3})e^{-u_{s3}/\mu_3} + A_3 \left[ \frac{3\sqrt{\pi}}{5}\text{erfc}(\sqrt{u_{s3}}) \right.$$
$$\left. + e^{-u_{s3}}\sqrt{u_{s3}}\left(u_{s3}^2 + \frac{7}{10}u_{s3} + \frac{6}{5}\right) \right], \qquad (8)$$

where $\text{erfc}(x)$ is the complementary error function. For speckles with a Gaussian transverse profile [$I(r) = Ie^{-(2\sqrt{\log 2}r/w_s)^2}$] and full width at half-maximum (FWHM) $w_s$, integration over $r$ gives the mean power in a speckle, $\langle P_s \rangle_{2D} = \langle I/I_0 \rangle_{2D} I_0 w_s \sqrt{\pi/\log 2}$ and $\langle P_s \rangle_{3D} = \langle I/I_0 \rangle_{3D} I_0 w_s^2 \pi/(4\log 2)$. Finally, the expected

number of speckles in two and three dimensions (2D and 3D), respectively, is

$$N = \frac{\sigma_b}{w_s \langle I/I_0 \rangle_{2D}} \sqrt{\frac{\log 2}{\pi}}, \quad (9)$$

$$N = \frac{\sigma_b}{w_s^2 \langle I/I_0 \rangle_{3D}} \frac{4 \log 2}{\pi}. \quad (10)$$

The single-speckle threshold ($I_{\text{thr,speckle}}$) generally depends on the speckle size, plasma conditions, and the instability under consideration. Here we focus on the absolute TPD instability, which can grow only in a narrow region near the quarter-critical density [30,31]. An analytic approximation can be developed by constructing a spatially localized solution out of the linear eigenmodes for a plane-wave drive laser propagating parallel to a linear density gradient along the $x$-direction, which have the form $n_e(\mathbf{x}, t) = u(x, t)e^{ik_y y + ik_z z} +$ c.c. [31]. In the simplest case in which the speckles are aligned with the density gradient, the transverse speckle width plays the dominant role in determining the single-speckle threshold, and we can neglect the impact of speckle length because the longitudinal ($x$-direction) mode width is typically smaller than the speckle length. Because the transverse eigenmode width is formally infinite, spatially localized growth requires a superposition of the linear eigenmodes. The transverse part of the linear eigenmodes are simply Fourier modes, so the spectral width of the superposition is inversely proportional to the spatial width. Accordingly, the spectral width of the transverse eigenmodes is approximately $\Delta k_\perp \approx 2\pi/w_s$ or $\Delta k_\perp/k_0 \approx 1/f_\#$ ($k_0 = 2\pi/\lambda_0$). An analytic approximation to the single-speckle thresholds is obtained from the plane-wave result by requiring absolute instability over the corresponding range of linear eigenmodes.

A straightforward generalization of the derivation in Ref. [31] to include eigenmodes outside the plane of polarization ($k_z \neq 0$) gives the threshold condition

$$\frac{\alpha}{2\beta^{1/2}} > \frac{(\psi + 1 + q_z/q_y)^2}{2\psi + 1 + q_z/q_y} \left( \frac{2\psi - 1 - q_z/q_y}{\psi} \right)^{1/2}, \quad (11)$$

where

$$\psi = -1 - \frac{q_z}{q_y} - \frac{1}{2 \times 3^{1/3} q_y \beta \xi} + \frac{\xi}{2 \times 3^{2/3}}, \quad (12)$$

$\xi = [18(1 + q_z/q_y)/(q_y\beta)]^{1/3}$,     $\alpha = 4k_0^2 v_0 L_n/\omega_0$,     $\beta = 9v_{te}^4 k_0^2/v_0^2\omega_0^2$, $q_i = (k_i/k_0)^2$, $L_n$ is the density scale length, $v_{te}$ is the electron thermal velocity, and $v_0$ is the electron oscillation velocity. $v_0$ is converted to intensity (in cgs units) using $I = \frac{cm_e^2\omega_0^2 v_0^2}{8\pi e^2} \sqrt{1 - \frac{n_{e0}}{n_c}}$, where $m_e$ is the electron mass, $c$ is the speed of light in vacuum, $n_{e0}$ is the background electron density, $e$ is the magnitude of the electron charge, and $n_c = \omega_0^2 m_e/4\pi e^2$ is the critical density for light with frequency $\omega_0$. Equation (11) was derived assuming $\beta \gg 1$, which is typically satisfied in ICF experiments.

Figure 2(b) shows the single-speckle thresholds as a function of speckle width for $L_n = 400$ $\mu$m, $T_e = 4$ keV, and $\lambda_0 = 0.405$ $\mu$m. The thresholds are normalized to the analytic plane-wave threshold [31]

$$I_{\text{thr,TPD}} = 0.658 \frac{c^4 m_e^2 \omega_0}{e^2 L_n} \frac{v_{te}^2}{c^2}. \quad (13)$$

The analytic results are compared to single-speckle calculations from the LPSE code, where the time-enveloped linearized electron-fluid equation [Eq. (2) in Ref. [32]] was solved pseudospectrally using an applied laser field. The thresholds were determined by running a series of simulations and using the bisection method to locate the threshold intensity (Appendix A of Ref. [32]). The important qualitative features that are apparent in both the analytic approximation and the LPSE results are the sharp increase in threshold at small speckle width and the considerable difference between the 2D and 3D thresholds. The sharp increase in the threshold occurs because linear eigenmodes with large $k_\perp$ have much higher thresholds than the small $k_\perp$ modes. Similarly, the large difference between the 2D and 3D thresholds results from the increased thresholds for the out-of-plane eigenmodes ($k_z \neq 0$).

Despite the qualitative success of the analytic model for the single-speckle threshold, it is not sufficiently accurate for quantitative threshold calculations. Accordingly, in the comparisons to full speckled-beam calculations that follow, a "semianalytic" version of Eq. (1) was used, where $I_{\text{thr,speckle}}$ is taken from nonlinear fits to the single-speckle LPSE results. This limits the generality of the results because it requires a series of single-speckle simulations for each $L_n$ and $T_e$. One additional correction that was not accounted for in the single-speckle threshold calculations was that the wavelength in a speckle is slightly longer than the laser wavelength because it corresponds to the projection of the component laser wave vectors along the speckle direction. The TPD threshold at fixed laser frequency is proportional to the wavelength, so this introduces a $1/\cos\theta$ correction to the single-speckle threshold. Finally, because of the sharp increase in threshold at small speckle widths, there are situations in which including only a subset of the beams (or, equivalently, a subregion of the beam aperture) will result in reduced thresholds. This is readily included in the model but does not impact any of the results that follow.

Figure 3 shows comparisons of Eq. (1) to various speckled-beam LPSE calculations. Figure 3(a) shows 2D calculations using a single beam with varying $f$-number at $L_n = 200$ $\mu$m, $T_e = 2$ keV and $L_n = 400$ $\mu$m, $T_e = 4$ keV, which are similar to the conditions in direct-drive ICF experiments on the OMEGA [33] and National Ignition Facility [13] lasers, respectively. The thresholds are higher in the longer-scale-length calculations because, for a given speckle width, the single-speckle threshold increases with increasing temperature and scale length.

Figures 3(b) and 3(c) show 3D instability thresholds for $L_n = 200$ $\mu$m, $T_e = 2$ keV and $L_n = 400$ $\mu$m, $T_e = 4$ keV, respectively, for three different beam configurations: (i) a single beam with varying $f$-number; (ii) six $f/6.7$ beams uniformly distributed on a cone relative to the $x$-axis with polar angle $\theta$ and azimuthal angle for the $m$th beam $\phi_m = 2\pi m/6$; and (iii) eight $f/6.7$ beams organized into two four-beam cones with polar angles $\theta$ and $\theta/2$ and azimuthal angles $\phi_m = 2\pi m/4$ and $\phi_m = 2\pi m/4 + \pi/4$, respectively. For the multibeam cases, the horizontal axis corresponds to an effective $f$-number given by the cone angle, $f_\# = 1/(2\tan\theta)$, and the beam polarizations were aligned. All three beam configurations give the same threshold to within statistical variations and are in good
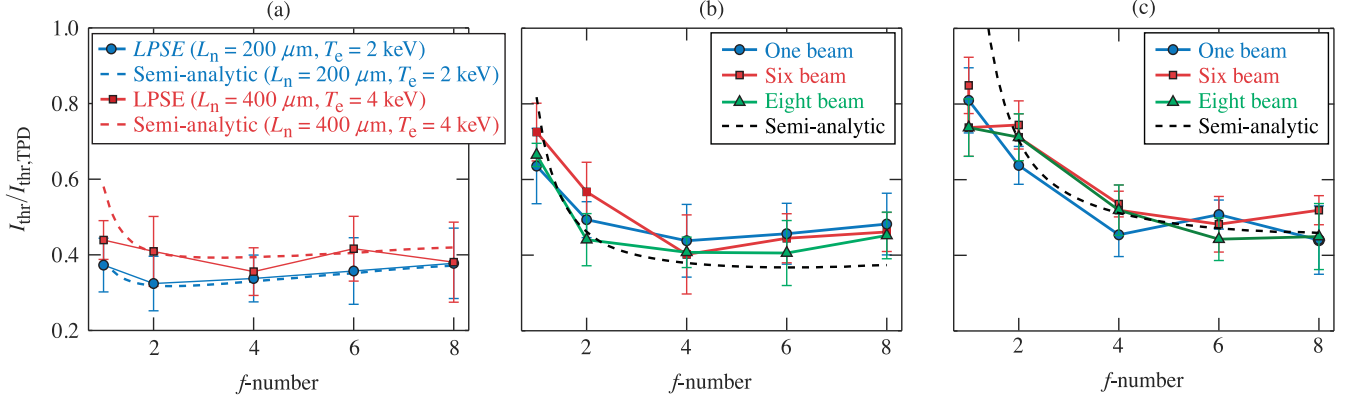
FIG. 3. Absolute TPD instability thresholds for speckled beams. (a) 2D results. (b),(c) 3D results for $L_n = 200$ $\mu$m, $T_e = 2$ keV and $L_n = 400$ $\mu$m, $T_e = 4$ keV, respectively. The dashed curves show the corresponding semianalytic results. The error bars correspond to the standard deviation from an ensemble of 20 (5) speckle realizations in 2D (3D).

agreement with the semianalytic model. This shows that the instability behavior is predominantly determined by the smallest (and highest-intensity) speckles and justifies the treatment of the cones of beams as a single beam with a small effective $f$-number.

The good agreement between the LPSE simulations and the semianalytic model is suggestive that the instability is in the single-speckle regime, but it is not definitive evidence. Here we can simply inspect the fields in the LPSE simulations and find that the instability growth is localized to a single-speckle in all cases but when $f_{\#} = 1$, $L_n = 400$ $\mu$m, and $T_e = 4$ keV, which is consistent with the fact that the semianalytic model diverges significantly from the LPSE results in that region.

The thresholds in Fig. 3 cannot be compared directly to experiments because they correspond to the average intensity required for absolute growth in a single speckle, which has an implicit volume dependence. Assuming single-speckle behavior, the formalism developed here can readily be applied to convert the threshold definition used in Fig. 3 to approximate an effective threshold for the average intensity $I_{\mathrm{thr},f}$ such that some fraction $f$ of the speckles are above threshold:

$$I_{\mathrm{thr},f} = \frac{\langle I_M/I_0\rangle I_{\mathrm{thr}}}{u_f},\tag{14}$$

where $u_f$ is obtained by numerically solving $P(I/I_0 > u_f) = f$ using the distributions in Eq. (3) or (4).

A direct comparison of these results can be made with the experimental results given in Ref. [7], where hot-electron production from a four-beam configuration with parallel polarizations (incident at $23°$ relative to the target normal) was compared to the single-beam case ($f_{\#} = 6.7$). The plasma conditions were similar to those in Fig. 3(b), and the authors state that the ratio of scale length to temperature was approximately constant ($L_n/T_e \approx 160$ $\mu$m/keV) over the range of intensities considered with $\sim 50\%$ of the incident laser energy reaching the quarter-critical surface. This corresponds to a vacuum plane-wave threshold intensity of $I_{\mathrm{thr,TPD}} = 2.5 \times 10^{14}$ W/cm$^2$. To make a threshold comparison, we assume that when somewhere between 1% and 10% of the speckles were above threshold [$f = 0.01$–$0.1$

in Eq. (14)], the measured hot-electron fraction was in the range $10^{-4}$–$10^{-3}$. Accordingly, the semianalytic model gives $I_{\mathrm{thr}}/I_{\mathrm{thr,TPD}} = 0.3 \pm 0.1$ and $1.0 \pm 0.2$ or vacuum threshold intensities of $0.8 \pm 0.3 \times 10^{14}$ and $2.5 \pm 0.5 \times 10^{14}$ W/cm$^2$ for the single- and four-beam cases, respectively. The corresponding experimental thresholds were $1.3 \pm 0.2 \times 10^{14}$ and $2.3 \pm 0.3 \times 10^{14}$ W/cm$^2$. LPSE predicts that both configurations should be in the single-speckle regime, which is corroborated by the good agreement between the prediction and the experiment in the four-beam case. Despite the significant (38%) underprediction of the single-beam threshold, we can be confident that those results were also in the single-speckle regime because of the large speckle size. Additionally, this discrepancy is not very surprising because the semianalytic model also underpredicts the LPSE results by $\sim 24\%$ for $f_{\#} = 6.7$, and all of the calculations presented here neglected electron-ion collisional damping, which would increase the predicted thresholds by $\sim 10\%$. LPSE calculations using the actual plasma conditions and beam geometry from the paper (and collisions) predict thresholds of $1.2 \pm 0.2 \times 10^{14}$ (one-beam) and $2.9 \pm 0.5 \times 10^{14}$ W/cm$^2$ (four-beam).

Reference [7] also included two-beam subsets of the four-beam configuration, which results in speckles that are narrow in the dimension parallel to the direction of separation but wide in the other dimension. For the case in which the polarization is aligned with the direction of separation, this is similar to the 2D geometry because the speckles are wide in the out-of-plane dimension. To within error, this gives the same predicted threshold as the single-beam 3D case, which was also true in the experiments.

Reference [12] has experiments that used two different beam configurations with the same effective $f$-number but different predicted common-wave thresholds. Although the use of polarization smoothing precludes a quantitative comparison, the measured thresholds were not sensitive to the configuration, which is consistent with the model developed here because configurations with the same effective $f$-number have the same predicted threshold.

These results have several important implications for experimental design: (i) The only way to increase thresholds by modifying beam geometry is to reduce the effective $f$-number. (ii) Thresholds can be increased by reducing the

peak speckle intensity (e.g., with polarization smoothing). (iii) Schemes that use reduced laser focal spot size to mitigate cross-beam energy transfer [34] will result in decreased TPD thresholds because concentrating the laser energy in near-normal-incidence beams results in a larger effective $f$-number. (iv) Speckle motion is more likely to have an impact on instability thresholds in the single-speckle regime.

We have shown that multibeam TPD often exhibits single-speckle behavior than can be understood in the context of an independent-hot-spot model. A procedure for deriving a semianalytic independent-hot-spot model was developed and applied to the absolute TPD instability, which shows good agreement with LPSE calculations. The approach can readily be applied to other instabilities and to include additional effects like polarization [27] and temporal smoothing [21,25]. Although there is no general procedure for determining the point of transition from single- to multispeckle behavior, it is clear that it will occur at smaller speckle sizes for more spatially localized instabilities such as absolute instabilities or weakly damped convective instabilities.

[1] S. Atzeni and J. Meyer-ter Vehn, *The Physics of Inertial Fusion: Beam Plasma Interaction, Hydrodynamics, Hot Dense Matter*, International Series of Monographs on Physics (Clarendon, Oxford, 2004)

[2] W. L. Kruer, *The Physics of Laser Plasma Interactions*, Frontiers in Physics Vol. 73 (Addison-Wesley, Redwood City, CA, 1988).

[3] R. S. Craxton, K. S. Anderson, T. R. Boehly, V. N. Goncharov, D. R. Harding, J. P. Knauer, R. L. McCrory, P. W. McKenty, D. D. Meyerhofer, J. F. Myatt, A. J. Schmitt, J. D. Sethian, R. W. Short, S. Skupsky, W. Theobald, W. L. Kruer, K. Tanaka, R. Betti, T. J. B. Collins, J. A. Delettrez, S. X. Hu, J. A. Marozas, A. V. Maximov, D. T. Michel, P. B. Radha, S. P. Regan, T. C. Sangster, W. Seka, A. A. Solodov, J. M. Soures, C. Stoeckl, and J. D. Zuegel, Phys. Plasmas **22**, 110501 (2015).

[4] Y. Kato, K. Mima, N. Miyanaga, S. Arinaga, Y. Kitagawa, M. Nakatsuka, and C. Yamanaka, Phys. Rev. Lett. **53**, 1057 (1984).

[5] C. Stoeckl, R. E. Bahr, B. Yaakobi, W. Seka, S. P. Regan, R. S. Craxton, J. A. Delettrez, R. W. Short, J. Myatt, A. V. Maximov, and H. Baldis, Phys. Rev. Lett. **90**, 235002 (2003).

[6] D. F. Dubois, B. Bezzerides, and H. A. Rose, Phys. Fluids B **4**, 241 (1992).

[7] D. T. Michel, A. V. Maximov, R. W. Short, S. X. Hu, J. F. Myatt, W. Seka, A. A. Solodov, B. Yaakobi, and D. H. Froula, Phys. Rev. Lett. **109**, 155007 (2012).

[8] P. Michel, L. Divol, E. L. Dewald, J. L. Milovich, M. Hohenberger, O. S. Jones, L. B. Hopkins, R. L. Berger, W. L. Kruer, and J. D. Moody, Phys. Rev. Lett. **115**, 055003 (2015).

[9] J. Zhang, J. F. Myatt, R. W. Short, A. V. Maximov, H. X. Vu, D. F. DuBois, and D. A. Russell, Phys. Rev. Lett. **113**, 105001 (2014).

[10] D. T. Michel, A. V. Maximov, R. W. Short, J. A. Delettrez, D. Edgell, S. X. Hu, I. V. Igumenshchev, J. F. Myatt, A. A. Solodov, C. Stoeckl, B. Yaakobi, and D. H. Froula, Phys. Plasmas **20**, 055703 (2013).

[11] J. F. Myatt, J. Zhang, R. W. Short, A. V. Maximov, W. Seka, D. H. Froula, D. H. Edgell, D. T. Michel, I. V. Igumenshchev, D. E. Hinkel, P. Michel, and J. D. Moody, Phys. Plasmas **21**, 055501 (2014).

[12] R. K. Follett, J. F. Myatt, J. G. Shaw, D. T. Michel, A. A. Solodov, D. H. Edgell, B. Yaakobi, and D. H. Froula, Phys. Plasmas **24**, 102134 (2017).

[13] M. J. Rosenberg, A. A. Solodov, J. F. Myatt, W. Seka, P. Michel, M. Hohenberger, R. W. Short, R. Epstein, S. P. Regan, E. M. Campbell, T. Chapman, C. Goyon, J. E. Ralph, M. A. Barrios, J. D. Moody, and J. W. Bates, Phys. Rev. Lett. **120**, 055001 (2018).

[14] R. K. Follett, J. G. Shaw, J. F. Myatt, D. H. Froula, and J. P. Palastro, Phys. Rev. E **101**, 043214 (2020).

[15] H. A. Rose and D. F. DuBois, Phys. Rev. Lett. **72**, 2883 (1994).

[16] H. A. Rose, Phys. Plasmas **2**, 2216 (1995).

[17] P. Mounaix, Phys. Rev. E **52**, R1306 (1995).

[18] L. Divol and P. Mounaix, Phys. Plasmas **6**, 4037 (1999).

[19] V. T. Tikhonchuk, C. Labaune, and H. A. Baldis, Phys. Plasmas **3**, 3777 (1996).

[20] V. T. Tikhonchuk, P. Mounaix, and D. Pesme, Phys. Plasmas **4**, 2658 (1997).

[21] P. Mounaix, L. Divol, S. Huller, and V. T. Tikhonchuk, Phys. Rev. Lett. **85**, 4526 (2000).

[22] D. Turnbull, A. V. Maximov, D. Cao, A. R. Christopherson, D. H. Edgell, R. K. Follett, V. Gopalaswamy, J. P. Knauer, J. P. Palastro, A. Shvydky, C. Stoeckl, H. Wen, and D. H. Froula, Phys. Plasmas **27**, 102710 (2020).

[23] P. Mounaix and L. Divol, Phys. Rev. Lett. **93**, 185003 (2004).

[24] R. J. Adler, *The Geometry of Random Fields*, Classics in Applied Mathematics (Society for Industrial and Applied Mathematics, Philadelphia, 2010).

[25] J. Garnier and L. Videau, Phys. Plasmas **8**, 4914 (2001).

[26] D. Pesme, S. Huller, J. Myatt, C. Riconda, A. Maximov, V. T. Tikhonchuk, C. Labaune, J. Fuchs, S. Depierreux, and H. A. Baldis, Plasma Phys. Control. Fusion **44**, B53 (2002).

[27] A. L. Cain, G. Riazuelo, and J. M. Sajer, Phys. Plasmas **18**, 082711 (2011).

[28] B. Eisenberg, Stat. Probab. Lett. **78**, 135 (2008).

[29] J. Garnier, Phys. Plasmas **6**, 1601 (1999).

[30] C. S. Liu and M. N. Rosenbluth, Phys. Fluids **19**, 967 (1976).

[31] A. Simon, R. W. Short, E. A. Williams, and T. Dewandre, Phys. Fluids **26**, 3107 (1983).

[32] R. K. Follett, J. G. Shaw, J. F. Myatt, C. Dorrer, D. H. Froula, and J. P. Palastro, Phys. Plasmas **26**, 062111 (2019).

[33] T. R. Boehly, V. A. Smalyuk, D. D. Meyerhofer, J. P. Knauer, D. K. Bradley, R. S. Craxton, M. J. Guardalben, S. Skupsky, and T. J. Kessler, J. Appl. Phys. **85**, 3444 (1999).

[34] I. V. Igumenshchev, W. Seka, D. H. Edgell, D. T. Michel, D. H. Froula, V. N. Goncharov, R. S. Craxton, L. Divol, R. Epstein, R. Follett, J. H. Kelly, T. Z. Kosc, A. V. Maximov, R. L. McCrory, D. D. Meyerhofer, P. Michel, J. F. Myatt, T. C. Sangster, A. Shvydky, S. Skupsky, and C. Stoeckl, Phys. Plasmas **19**, 056314 (2012).